atmosphere

MDPI

Article

Inverse Modeling of Nitrogen Oxides Emissions from the 2010 Russian Wildfires by Using Satellite Measurements of Nitrogen Dioxide

Evgeny V. Berezin [1], Igor B. Konovalov [1,*] and Yulia Y. Romanova [2,*]

[1] Institute of Applied Physics, Russian Academy of Sciences, 46 Ulyanov Street, Nizhniy Novgorod 603950, Russia; e.berezin@appl.sci-nnov.ru

[2] Institute for Physics of Microstructures, Russian Academy of Sciences, Afonino, 7 Academicheskaya Street, Nizhniy Novgorod 603087, Russia

* Correspondence: konov@appl.sci-nnov.ru (I.B.K.); jul@ipm.sci-nnov.ru (Y.Y.R.); Tel.: +7-831-416-4902 (I.B.K.)

Academic Editor: Anthony R. Lupo

Received: 6 September 2016; Accepted: 12 October 2016; Published: 16 October 2016

Abstract: Observational constraints to biomass burning (BB) NO_x emissions as provided by satellite measurements of nitrogen dioxide (NO_2) critically depend on quantitative assumptions regarding the atmospheric NO_x lifetime. In this study, we investigated NO_x emissions from the extreme wildfires that occurred in the European part of Russia in summer 2010 by using an original inverse modeling method that allowed us to avoid any a priori assumptions regarding the NO_x lifetime. The method was applied to the tropospheric NO_2 columns retrieved from the measurements performed by the OMI satellite instrument, while the relationship between BB NO_x emissions and tropospheric NO_2 columns was simulated with the CHIMERE mesoscale chemistry transport model. Our analysis indicated that this relationship depends strongly on BB emissions of volatile organic compounds and that a dependence of the effective NO_x lifetime on the NO_x fluxes can be essentially nonlinear. Our estimates of the total NO_x emissions in the study region are found to be at least 40% larger compared to the respective data from the GFASv1.0 and GFED4.1s global fire emission inventories.

Keywords: nitrogen oxides; wildfires; satellite measurements; chemistry transport model; inverse modeling; biomass burning emissions

1. Introduction

Nitrogen oxides (NO_x = NO + NO_2) are important atmospheric constituents affecting climate processes and air quality specifically by serving as precursors of tropospheric ozone [1,2] and influencing secondary aerosol formation [3,4]. One of the significant sources of NO_x on a global scale is associated with open biomass burning (BB): it is estimated that BB provides around 15% of total NO_x emissions globally [5]. On a regional scale, BB NO_x emissions can play a predominant role in the oxidation processes leading to ozone formation inside smoke plumes from wildfires [6] over other NO_x sources and provide a major contribution to NO_2 column amounts over fire spots [7].

Despite the important role played by BB NO_x emissions in atmospheric processes, the current knowledge of the amounts of NO_x emitted into the atmosphere from wildfires is insufficient. Available BB NO_x emission estimates provided by fire emission inventories (e.g., [8,9]) based on indirect measurements of the amounts of biomass burned have mostly not been validated against atmospheric measurements and are likely to be rather uncertain as indicated by a diversity of the NO_x emission factor values involved in such inventories and reported in literature for similar types of vegetation cover [10]. Validation of BB NO_x emission estimates is more difficult compared to validation of BB emissions of some other species (such as, e.g., CO) particularly due to high reactivity and a

relatively short atmospheric lifetime of NO_x, leading to a strong variability of NO_x concentrations both in space and time.

Nonetheless, several studies [7,11–14] have recently examined the relationship between the satellite-retrieved fire radiative power (FRP) and the tropospheric NO_2 columns over fire spots and reported reasonable estimates of the fire emission rate (FER) [7,11] or the emission coefficient (EC) [12–14], both of which allow one to calculate NO_x emissions, given the observed values of FRP. The measurement-based estimates of FER or EC for different regions and different types of biophysical model applications (BioMA) are useful, as they provide insight into the capability of available parameterizations to capture spatial and temporal variability of NO_x emissions. However, such estimates are presently rather uncertain, particularly because they involve explicit quantitative assumptions regarding the NO_x lifetime and NO_2/NO ratio. For example, it has been argued [13] that as the NO_x lifetime is likely to vary across individual fire plumes between 2 and 6 h, the estimates of EC can be uncertain at least by a factor of 3.

In this study, we also use FRP and NO_2 columns derived from satellite measurements, but unlike the previous studies, we do not make any explicit assumptions on the NO_x lifetime and NO_2/NO ratio. Instead, we follow the inverse modeling approach that has earlier been successfully used (e.g., [15–18]) to estimate anthropogenic NO_x emissions. Within this approach, the relationship between NO_2 columns and NO_x emissions can be simulated by a chemistry transport model, and the NO_x emissions (or related emission parameters) as well as the NO_x lifetime can be estimated by fitting simulated NO_2 columns to satellite data. The goals of our study were (1) to examine feasibility of using an inverse modeling approach to estimate BB NO_x emissions in a region affected by numerous and intense wildfires; and (2) to assess the impact of chemical nonlinearities on the relationship between NO_x emissions from wildfires and corresponding NO_2 columns over such a region. We focused on the disastrous mega-fire event that took place in the European part of Russia in 2010. Emissions of some pollutants (such as CO and aerosol) from the Russian 2010 fires were already investigated using inverse methods (e.g., [19–21]), but, to the best of our knowledge, there have yet been no similar studies focusing on NO_x emissions from those fires.

2. Data and Method

2.1. Input Data

2.1.1. Satellite Data

We used tropospheric NO_2 column amounts retrieved from measurements of visible and ultraviolet back scattered radiation by the Ozone Monitoring Instrument (OMI) [22] onboard the NASA EOS Aura satellite and provided by KNMI as the DOMINO version 2 data product [23,24]. OMI provides global coverage daily at the 13×24 km^2 nominal spatial resolution; the measurements are taken in the early afternoon, as the Aura satellite operates in a sun-synchronous polar orbit with an equator crossing at 13:45 LST. The DOMINO version 2 data product was evaluated against ground-based (MAX-DOAS) measurements [25], and only a minor negative bias (~10%) was found in the satellite data. NO_2 data retrieved from the OMI measurements (although with slightly different algorithms) were found to be useful in earlier studies of BB NO_x emissions [7,11,12,14].

Following recommendations of the data providers, potentially biased data retrieved for the scenes with the cloud fraction and surface albedo exceeding 30% and 0.3%, respectively, were disregarded. The details of the retrieval algorithm can be found elsewhere [23]. Note that the tropospheric NO_2 column retrieval procedure does not explicitly account for optical effects of BB aerosol. However, such effects were taken into account and corrected for in the same way as similar effects associated with clouds. Scenes strongly contaminated by cloud or aerosol were discarded, and so the bias is likely to remain limited (<20%) [26]. The orbital NO_2 data available for the study period that spans from 15 July to 16 August 2010 were projected onto a 0.5 by 0.5 degree rectangular grid covering the study region (48°N–66°N; 20°E–56°E). Any data falling to the same grid on the same day were averaged.

As a primary source of information on NO_x emissions from fires, we used the Fire Radiative Power (FRP) data [27,28] retrieved from satellite measurements of infrared radiation with the MODIS instruments operating onboard the Aqua and Terra satellites. Both the Aqua and Terra satellites are in sun-synchronous polar orbits with corresponding equator overpass times of 13:30 and 10:30 LST (at daytime) and 01:30 and 22:30 LST (at nighttime). We used the standard MODIS Level 2 "thermal anomalies & fire" (MOD14 and MYD14, Collection 5) data product available free from the NASA Land Processes Distributed Active Archive Center [29]. The data were provided for each satellite overpass at the nominal 1×1 km^2 resolution. The same data have been widely used (e.g., [7,9,21]) to study fire emissions, and details about the retrieval algorithm and potential uncertainties can be found elsewhere [27].

Finally, our analysis involved satellite retrievals [30] of aerosol optical depth (AOD) at a 550 nm wavelength. The measurements were also performed by the MODIS instruments onboard Aqua and Terra satellites. We used the Level 3 MYD08_D3/MOD08_D3 data product obtained from the NASA Giovanni-Interactive Visualization and Analysis system [31] in the framework of an earlier study [21]. The data had the spatial resolution of 1 by 1 degree and the temporal resolution of one day.

2.1.2. Simulation Data

Along with NO_2 data derived from satellite measurements, we used NO_2 columns simulated with the CHIMERE chemistry transport model (CTM) [32]. The CHIMERE CTM is a typical Eulerian three-dimensional model enabling simulations of air pollution on various scales, from urban to continental ones. It takes into account major physical and chemical processes (including over 300 chemical and photochemical reactions) affecting the evolution of ~80 gaseous species in the lower atmosphere. It also enables simulations of aerosol species but simulated aerosol concentrations were not used in this study. In-detail descriptions of the model structure and of parameterizations of physical and chemical processes is available elsewhere [32]. The model documentation and the source code can be downloaded from the CHIMERE website [33]. CHIMERE was successfully used in a number of studies, including those dedicated to investigations of atmospheric effects of wildfires (e.g., [19,21,34,35]).

The CHIMERE configuration was the same as in a previous study [21] of the atmospheric impacts of the 2010 Russian wildfires, which was focused on simulation of BB aerosol. Specifically, the simulations were performed with a horizontal resolution of $0.5^\circ \times 0.5^\circ$ with the model grid covering most of European Russia and a portion of Eastern Europe (48°N–66°N; 20°E–56°E). In vertical, the model grid had 12 levels, with the top of the upper level fixed at 200 hPa.

Fire emissions were calculated and introduced into CHIMERE by using the emission model that had been successfully used and described in detail earlier [19,21,36]. Briefly, it assumes that the BB emission rate, E^s, of a species, s, in a given grid cell of the horizontal domain in an hour, t, is proportional to the daily mean FRP values, ϕ_d, that were inferred from daily maximum FRP values derived from the MODIS measurements (see Section 2.1.1) for a given grid cell:

$$E^s(t) = \alpha \Phi_d \sum_l \beta_l^s \rho_l h_{el}(t) c \quad (1)$$

where α is a conversion factor from FRP to dry BB rate, which is referred to below also as the FRP-to-BBR conversion factor and for which a "reference" value, α_r, of 0.368 kg·s^{-1}·MW^{-1} is adopted, taking into account the experimental data [37], β_l^s are the emission factors for a species s and a land cover type l, ρ_l is the fraction of the land cover type l, h_{el} is the diurnal variation of fire emissions, and c is an ad hoc correction factor which was calculated (see [19,21]) using the measured AOD values and was intended to compensate for a possible attenuation of FRP measured from satellites by very heavy smoke and also to account (at least partly) for emissions from peat fires. The emission factor values, β_l^s, for the three aggregated vegetative land cover types (forest, grassland, and agricultural land) were taken to be the same as in our previous study (see [21] and Table 2 therein). The emission diurnal cycle was

also adopted from the previous study (see [21] and Figure 1 therein), where it had been derived for the study region from the FRP measurements using a method developed earlier [36]. The emissions were distributed in the vertical direction by using a well-known parameterization [38] of the maximum injection height of BB emission as a function of FRP and the boundary layer height. The emission profiles were calculated for each grid cell and each hour by assuming that BB emissions corresponding to individual fire pixels are uniformly distributed from the ground up to the altitude corresponding to the maximum injection height.

Note that our fire emission model given by Equation (1) disregards possible variations of the FRP-to-BBR conversion factor both in space and time. It also does not explicitly take into account emissions from peat fires which are not visible from space. These simplifications are mainly due to the lack of observational information about such variations. Available estimates of α for different vegetation land cover types [9] are based on emission inventory data and, for this reason, were not quite suitable for our study based on the inverse modeling approach.

A noteworthy feature of our simulations is that hourly values of the photolysis rates were calculated "offline" for each grid cell and hour using the TUV model [39] and the satellite AOD data described in Section 2.1.1 (see also [19] for details of our calculations). CHIMERE runs were driven with meteorological data obtained from the WRF-ARW (v. 3.6) model [40]. Further details on meteorological data, anthropogenic and biogenic emission data, and boundary and initial conditions used in the CHIMERE runs performed in this study can be found elsewhere [21].

The hourly BB NO_2 concentration data obtained from the CHIMERE runs were matched in time and space to the satellite NO_2 data and integrated vertically by applying the averaging kernels [41]. The averaging kernels provide information on contribution of different atmospheric layers to the tropospheric NO_2 column amounts retrieved from the OMI measurements and were available as a part of the DOMINO data product. The hourly BB NO_2 concentrations available for the same day and grid cell were averaged.

The model was run for the period from 12 July to 16 August 2010 both with and without fire emissions. Only the difference of nitrogen oxides concentrations from the two "twin" runs was considered in this study in order to minimize an impact of probable biases in biogenic and anthropogenic emissions on our estimates: such a difference was considered as a contribution of BB emissions to the nitrogen oxides concentrations. The first three days of the model runs were withheld from the analysis for the model's spin-up. The three-day spin-up was found to be sufficient in the case considered for evaluation of the BB fraction of tropospheric NO_2 columns, since there had been no significant fire emissions in the study region before the initial date of the simulation.

2.2. Method

Estimation of NO_x emissions was based on a general approach established in previous studies [19,21,36]. The idea is to optimize one or more parameters of the fire emission model by fitting modeled concentrations of a species considered to respective observations. Following one of the previous studies [21], we optimized the FRP-to-BBR conversion factor (α) by assuming (in accordance to Equation (1)) that the same value of that factor is applicable to any types of vegetation land cover. Although, in reality, it is not necessarily true, large uncertainties in the measurement and simulation data prevent us from obtaining estimates of α separately for individual biome types. Variability of the true values of α is expected to be taken into account in the confidence intervals for our estimates.

In this study, the optimal value of α, α_{opt}, was inferred by fitting the NO_2 columns simulated with the CHIMERE model to those derived from the OMI observations:

$$\alpha_{opt} = \mathrm{argmin} \sum_{i=1}^{Nd} \left(C_o^i - C_b^i - C_{mf}^i \right)^2 \quad (2)$$

where C_o are the observed tropospheric NO_2 columns, C_b are the background parts of the tropospheric NO_2 columns (that is, the tropospheric NO_2 column amounts which would be present in the

atmosphere if there were no fires and which were estimated as explained below), C_{mf} are the simulated tropospheric column amounts of NO_2 originating from fires and i is the index of a day. The NO_2 column amounts (C_o, C_b, C_{mf}) involved in Equation (2) are the averages of the corresponding spatially-distributed data for a given day over the study region. Note that the spatial averaging was performed in order to minimize the impact of possible random uncertainties in the spatial variations of the NO_2 columns (due to, e.g., errors in the spatial distributions of fire emissions evaluated using Equation (1)) on our emission estimates.

To estimate the background NO_2 columns in a given grid cell (i) and in a given day (d), we considered the tropospheric NO_2 columns derived from the OMI measurements for the same grid cell but for another day chosen from the period from 15 July to 19 July 2010, when, according to our simulations, a contribution of fires to the mean NO_2 columns over the study region was negligible. If such "background" data were available for more than one day, a nearest, to d, day was selected. On the other hand, if there were no observational data for any of the days in the indicated period, then the given grid cell i was excluded from further analysis.

Importantly, estimation of the background NO_2 columns in such a way does not rely on the accuracy of the simulations of NO_2 columns in the background conditions. This allows us to minimize the effect of possible biases (due to, e.g., uncertainties in anthropogenic and biogenic NO_x emissions, as well as in the boundary conditions for NO_x and related species) in the background simulations with CHIMERE for the study region [42,43] on our estimates. Note that C_{mf} involved in Equation (2) was obtained as the difference between the results of two "twin" model runs with and without fire emissions (as mentioned in Section 2.1.2), and so C_{mf} also could not be directly influenced by possible inaccuracies of the simulations for the background conditions. Furthermore, the analysis of our results (see Section 3.3 below) does not show any evidence that the dependence of C_{mf} on BB NO_x emissions is significantly affected by the background conditions in an indirect way (e.g., through chemical interactions) either.

Equation (2) was resolved iteratively. In each iteration, C_{mf}, was assumed to depend on BB NO_x emissions (and, thus, on α) linearly, that is:

$$C_{mf|\alpha=\alpha^{(n)}} \cong \frac{\alpha^{(n)}}{\alpha^{(n-1)}} C_{mf|\alpha=\alpha^{(n-1)}} \quad (3)$$

where $\alpha^{(n)}$ and $\alpha^{(n-1)}$ are values of the conversion factor in two consecutive iterations, n is the iteration index and the symbol "|" denotes conditioning. After substituting $\alpha^{(n)}$ (instead of α_{opt}) and C_{mf} given by Equations (3) into (2), the latter can be resolved analytically:

$$\alpha^{(n)} = \alpha^{(n-1)} \left(\sum_{i=1}^{i=Nd} C^{i2}_{mf|\alpha=\alpha^{(n-1)}} \right)^{-1} \sum_{i=1}^{i=Nd} (C^i_o - C^i_b) C^i_{mf|\alpha=\alpha^{(n-1)}} \quad (4)$$

In this study, the first iteration (based on the initial model run) was performed with the reference value of the conversion factor, α_r (see Section 2.1.2). Three iterations were found to be sufficient in order to ensure that $\alpha^{(n)}$ is converged to the optimal estimate of α with a relative numerical uncertainty of less than 5%.

Confidence intervals for α_{opt} were evaluated by means of a Monte Carlo experiment based on the bootstrapping method [44]. Specifically, the simulations performed with the optimal value of α were used to represent the "true" values of the BB fraction of the tropospheric NO_2 columns. The corresponding "observed" values were generated by sampling random errors from the residuals of the modeled (optimal) data for the NO_2 columns (see the right-hand part of Equation (2)) and adding them to such "true" values. The re-sampling procedure and estimation of α_{opt} (assuming a linear dependence of $\boldsymbol{C}_{mf}$ on α) were repeated 1000 times. The confidence intervals were evaluated (and are reported below) in terms of the 95th percentile. In this way, we took into account any model and measurement errors contributing to the cost function involved in the right-hand part of Equation (1). Such errors may be due to various non-systematic uncertainties in the retrieval procedure used to

derive tropospheric NO_2 columns from the OMI measurements [23,26,45], as well due to transport errors in our model. A part of the uncertainties taken into account in the confidence intervals for α_{opt} may be associated with our fire emission model (see Section 2.1.2), specifically with the simplifying assumptions concerning the FRP-to-BBR conversion factor as well as with possible inaccuracies of the injection height, with variability of the emission factors and with inaccuracies in the input FRP data. Indeed, it seems reasonable to expect that the errors associated with the emission model varied from day to day during the study period, reflecting temporal and spatial variations in the burning conditions and in the types and density of fuel.

It should be noted, however, that the confidence intervals reported below cannot fully account for systematic errors (biases) both in the OMI retrieval and in our simulations. Such biases may, in particular, be due to a probable underestimation of the NO_2 columns retrieved for the strongly polluted scenes. The biases may also be due to possible inconsistencies between the vertical distribution of NO_2 in the real atmosphere and the vertical profiles used in the retrieval procedure [45] and predicted by CHIMERE in this study. Evaluation of such systematic errors and their effects on the corresponding NO_x emission estimates is a challenging task that goes beyond the scope of this study.

Since the tropospheric NO_2 columns derived from satellite measurements provide information only on NO_x emissions, there is an issue concerning specification of BB emissions of other species (such as CO and volatile organic compounds, VOCs). As the main option, we used the same values of the conversion factor to calculate the BB emissions of all model species. This estimation case is labeled below as "VOCbyNO_x". However, as it was pointed out earlier [21,36], estimates of α derived from measurements of different species may be different, partly due to uncertainties in the assumed emission factors. Therefore, as another option, we calculated the BB emissions of CO and VOCs by using the value of α optimized in a previous study [21] against ground-based measurements of CO concentrations in the Moscow region: this CO-measurement-based value of α had been found to be a factor of 1.88 larger than its reference value α_r. The second estimation case is labeled below as "VOCbyCO".

Note that the estimation method described above is similar but not identical to those employed in the preceding studies [21,36] where satellite measurements and the CHIMERE model were used to constrain emissions of CO and aerosol from wildfires in Russia. The differences (that will not be discussed here in detail) are mainly due to the fact that CO and aerosol are much less reactive species compared to NO_x. Some specific assumptions (e.g., those concerning the origin of possible systematic uncertainties in simulated data) involved in the preceding studies were no longer valid in the case considered in this study and should have been avoided. For example, it was assumed that the bias in the simulated CO columns in the background conditions was mainly due to errors in the boundary conditions: accordingly, it was estimated by averaging the differences between the CO columns from the simulations and measurements over a number of grid cells and days representing similar environment conditions. In contrast, errors in the corresponding NO_2 columns may predominantly come from uncertainties in the biogenic and anthropogenic emissions specified in the model; furthermore, such errors are likely to strongly vary both in time and space because of a short lifetime of NO_x. Consequently, estimation of BB NO_x emissions using exactly the same methods as those employed in the previous studies turned out to be infeasible, and such methods had to be modified accordingly. The major difference is that here we estimate the background NO_2 columns directly from the measurement data and thus avoid the problem of estimating the bias in the corresponding simulated data.

To study a potential impact of chemical nonlinearities on BB NO_x emission estimates based on satellite measurements, we performed several additional model runs using BB emissions calculated with different values of the conversion factor. Specifically, the reference value of the conversion factor was scaled with a factor ranging from 0. 5 to 2, and the resulting values were used in Equations (3) and (4) as the "zero-order" estimate, $\alpha^{(0)}$, to obtain the "first-order" estimate (constrained by satellite

measurements according to Equation (2)) of the conversion factor, $\alpha^{(1)}$. Furthermore, we evaluated the effective lifetime of NO_x, τ_{nox}, corresponding to each value of $\alpha^{(0)}$ as follows:

$$\tau_{nox} = \left(\sum_{i=1}^{Nd}\sum_{j=1}^{Nc}\theta^{ij}e^{ij}\right)^{-1}\sum_{i=1}^{Nd}\sum_{j=1}^{Nc}\theta^{ij}v^{ij}, \quad (5)$$

where e^{ij} are the BB NO_x emission rates (g·hour^{-1}) in a grid cell j (in the horizontal domain) and in a day i, v^{ij} are values (simulated by the CHIMERE model) of the tropospheric column amounts of NO_x originating from wildfires (g), N_c and N_d are the total numbers of grid cells and days in the study region and period, and θ^{ij} is the selection operator—which is equal to unity if the measurement data for a given grid cell and day is available and to zero otherwise.

Equation (5) assumes that the evolution of the total (integral) amount of NO_x from BB burning over the study region can be roughly approximated by a simple balance equation describing the loss of NO_x as a first order decay process, with the rate expressed as $\tau_{nox}{}^{-1}$. The definition given by Equation (5) is based on the known concept [46] of the mean lifetime of an atmospheric substance and follows from a consideration of a simple balance equation for NO_x originating from fires (NO_x^f NO_x^f), describing the loss of NO_x^f as a first order decay process in each model grid cell in the three dimensional domain:

$$\frac{d[NO_x^f]}{dt} = (F_{in} - F_{out}) + (E - L[NO_x^f]), \quad (6)$$

where the square brackets denote the mass concentration of NO_x^f, F_{in} and F_{out} are the fluxes of NO_x^f in and out of the given grid cell, respectively, E is the local BB NO_x emission (or injection) rate, and L is the rate of losses of NO_x^f due to chemical and deposition processes. Note that the inverse of L gives an estimate of the "instant" lifetime of NO_x^f with respect to chemical and deposition processes in a given grid cell. After (i) averaging both the left and right parts of Equation (6) over the study region (both in the horizontal and vertical directions) and the study period; (ii) taking into account that concentration of NO_x^f approaches zero both at the beginning and at the end of the study period; (iii) disregarding the integral flux of NO_x^f from the study region (over which the persistent blocking anticyclone was developed in summer 2010 [47]); and (iv) multiplying both parts of the equation with the average amount of NO_x^f, we arrive to the following approximate relationship:

$$\left\langle L[NO_x^f]\right\rangle^{-1}\left\langle [NO_x^f]\right\rangle \approx \langle E\rangle^{-1}\left\langle [NO_x^f]\right\rangle, \quad (7)$$

where the angle brackets denote the average quantities. We further note that the term on the left-hand side of Equation (7) has the meaning of the mean NO_x^f lifetime evaluated as the inverse of the weighted average of L (with local NO_x^f concentrations being the weights), while the term on the right-hand part of Equation (7) is analogous to the term on the right-hand part of Equation (5). The main difference between Equation (7) and Equation (5) is that the latter includes only those values of the NO_x^f concentrations and BB NO_x emissions that correspond in space and time to the available OMI observations. Therefore, the effective lifetime, τ_{nox}, defined according to Equation (5) can be regarded as an approximation for the NO_x^f lifetime given by Equation (7).

Note that we considered only those values of NO_x^f that have counterparts in the satellite data, because the primary purpose of evaluation of τ_{nox} in this study was to investigate the effects of chemical nonlinearities on the BB NO_x emission estimates that can be derived from satellite measurement using either our method or simpler techniques involving a priori assumptions regarding the NO_x lifetime [12–14]. Note also that the relationship between $\alpha^{(1)}$ and $\alpha^{(0)}$ depends not only on the NO_x lifetime but also on the NO_2/NO ratio: this ratio, in turn, depends on ozone concentration and can be affected by changes in the NO_x emissions. In addition, unlike τ_{NOx} calculated using Equation (5), estimation of $\alpha^{(1)}$ partly takes into account BB NO_x emissions in grid cells (days) for which the

measurement data are not available. Therefore, the dependence of τ_{nox} on $\alpha^{(0)}$ cannot fully characterize that of the NO_2 columns retrieved from OMI measurements on the BB NO_x emission rate in the study region and period. Nonetheless, we believe that the estimates of τ_{nox} provided below can be helpful in characterizing the processes determining the relationship between the NO_2 columns and NO_x emissions. Furthermore, such estimates can eventually contribute to reducing uncertainties associated with FER or EC estimates [7,11–14] based on the analysis of the empirical relationships between FRP and tropospheric NO_2 columns. However, we do not recommend using our estimates of τ_{nox} outside of this specific context.

3. Results

3.1. Estimation of the FRP-to-BBR Conversion Factor

Estimation of the conversion factor (as explained in the previous section) is based on the analysis of daily time series of spatially averaged NO_2 columns derived from the OMI measurements (C_o) and simulated with the CHIMERE model (C_{mf}) and involves evaluation of the background fraction (C_b) of the tropospheric NO_2 columns. The corresponding time series are presented in Figure 1, along with the time series of the difference of C_o and C_b. Examples of underlying daily values of tropospheric NO_2 columns (specifically, on 29 July and 8 August) spatially distributed inside of the study region are shown in Figure 2. Note that values of C_{mf} shown in Figures 1 and 2 were calculated with the conversion factor equal to its reference value α_r specified above (see Section 2.1.2). Note also that the spatial distributions of CO and aerosol on the same days were considered in a preceding study [21].

As is evident from Figure 1, the simulations tend to overestimate the BB part of NO_2 columns (that is the difference of C_o and C_b), although the model captures, to a significant extent, the temporal variability of NO_2 column amounts from wildfires (specifically, the correlation coefficient exceeds a value of 0.75). The fact that, for some days, C_b is larger than C_o indicates that there may be considerable uncertainties in our estimates of background NO_2 values as well as in the original satellite NO_2 data. We assume that such uncertainties are mostly random in nature (varying from day to day) and thus are taken into account in the confidence intervals of our emission estimates reported below.

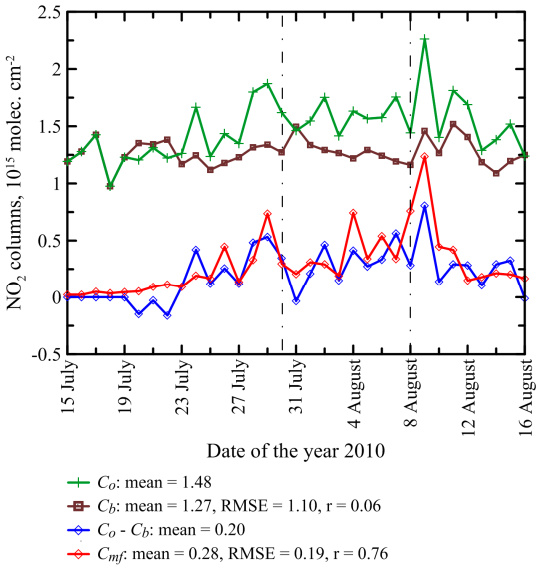

Figure 1. Time series of the daily NO_2 column amounts averaged over the study region. C_o: the tropospheric NO_2 columns retrieved from OMI measurements; C_b: a background part of tropospheric NO_2 columns; C_{mf}: the simulated tropospheric column amounts of NO_2 from wildfires. The vertical dash-dot lines mark the data for 29 July and 8 August. The RMSE and the correlation coefficient indicated in the figure legend for C_b and C_{mf} were calculated relative to C_o and $C_o - C_b$, respectively.

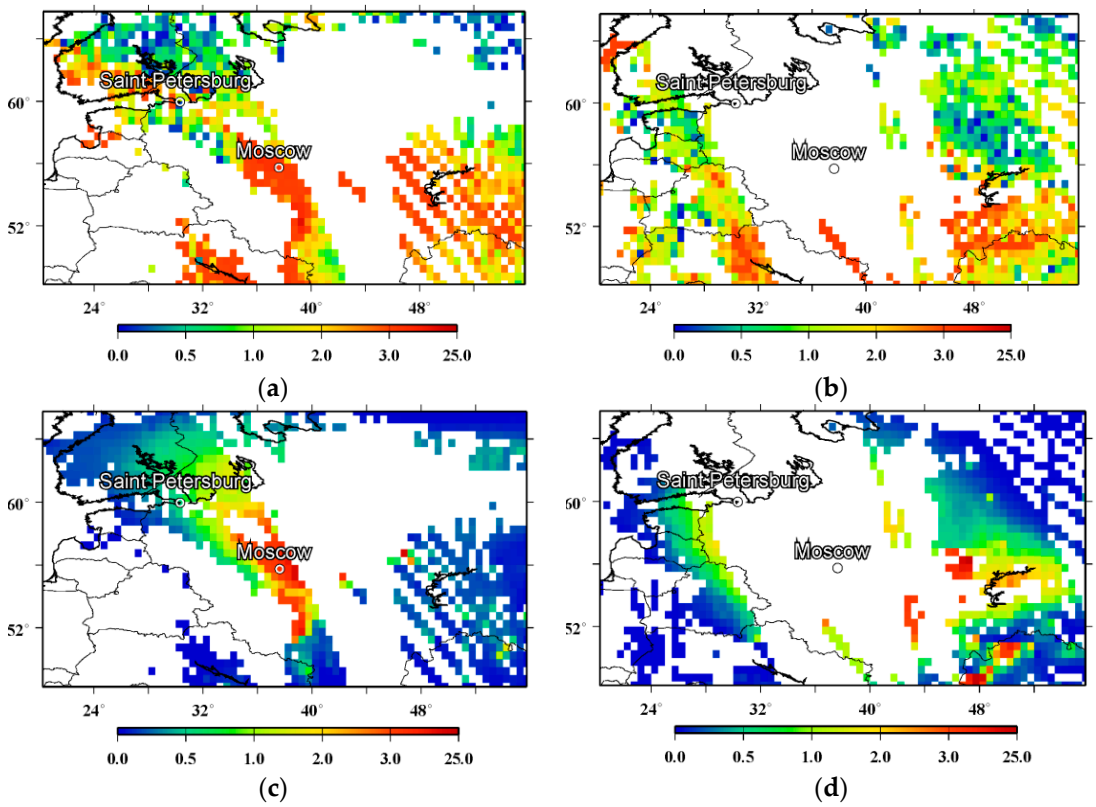

Figure 2. (**a**,**b**) Spatial distributions of the tropospheric NO_2 columns (10^{15} molec.·cm^{-2}) derived from the OMI measurements on 29 July and 8 August 2010; (**c**,**d**) the tropospheric NO_2 column amounts originated from wildfires, according to the simulations using the reference value of the FRP-to-BBR conversion factor. Note that the simulation data were processed with the averaging kernels from the OMI retrievals and are, accordingly, shown only where the measurement data were available.

Examples of spatial distributions of NO_2 columns shown in Figure 2 indicate that the NO_2 retrievals for many scenes in the study region and period were missing (apparently, due to interference of BB aerosol that is "shielding" the radiation coming to a satellite from the boundary layer). Nonetheless, many moderately polluted scenes showing considerable NO_2 amounts which, according to our simulations, originated from wildfires can still be seen in the OMI retrievals.

Figure 3 presents the conversion factor estimates, $\alpha^{(n)}$, that were obtained according to Equations (2)–(4) by using the simulations in which BB emissions were calculated with the assumed conversion factor values, $\alpha^{(n-1)}$. For convenience, values of both $\alpha^{(n)}$ and $\alpha^{(n-1)}$ are normalized to the reference value of the conversion factor, α_r. Most of the estimates shown in Figure 3 illustrate results of the first iteration (n = 1), except for the optimal estimates (circumvented by black circles in Figure 3) of α (α_{opt}) that were obtained as a result of the third iteration (n = 3). The estimates were obtained separately for the two cases ("VOCbyNO$_x$" and "VOCbyCO") that involve the different assumptions regarding the BB emissions of VOCs and CO. If the relationship between the simulated NO_2 columns and the BB NO_x emissions were linear, then any value of $\alpha^{(n-1)}$ would yield the same value of $\alpha^{(n)}$, or, in other words, $\alpha^{(n)}$ would be independent of $\alpha^{(n-1)}$. Our results show that $\alpha^{(n)}$ is indeed very weakly (positively) dependent on $\alpha^{(n-1)}$, but only for the case "VOCbyNO$_x$". A more pronounced (decreasing) dependence of $\alpha^{(n)}$ on $\alpha^{(n-1)}$ is found for the case "VOCbyCO". Overall, our results shown in Figure 3 indicate that the effects of chemical nonlinearities on the relationship between the BB emissions and tropospheric NO_2 columns in the situation considered cannot be disregarded, at least without certain constraints on VOCs emissions, although these effects are not very strong. In particular, the increase of $\alpha^{(0)}$ from 0.5 to 2 (that is, by a factor 4) in the "VOCbyCO" case resulted in the decrease of $\alpha^{(1)}$

from 0.96 to 0.67 (that is, only by about 30 percent), which is an effect of the corresponding increase (by a factor of ~1.3) of the ratio of the mean BB NO_2 column amounts and NO_x emission rates in the respective simulations.

It is especially noteworthy that the sensitivity of the optimal estimates of α to changes in BB VOC emissions turned out to be relatively small: specifically, while BB VOCs emissions for the "VOCbyCO" case were almost a factor of 3 larger than for the "VOCbyNO_x" case (when $\alpha = \alpha_{opt}$), the optimal estimate of the conversion factor is found to be only 17 percent larger for the former case (0.298 ± 0.053 kg·s^{-1}·MW^{-1}) than that for the latter one (0.254 ± 0.045 kg·s^{-1}·MW^{-1}). Unfortunately, there are presently no data that would allow us to characterize the uncertainty of the regionally averaged emission factors for VOCs, although such uncertainty is likely much smaller than the standard deviation (close to 100% [48]) of individual emission factor measurements. Note that systematic uncertainties in our estimates of α due to biases in the emission factors for VOCs are probably only partly accounted for in the confidence intervals for these estimates, to an extent as such uncertainties are associated with errors in the simulated daily variations of the tropospheric NO_2 columns.

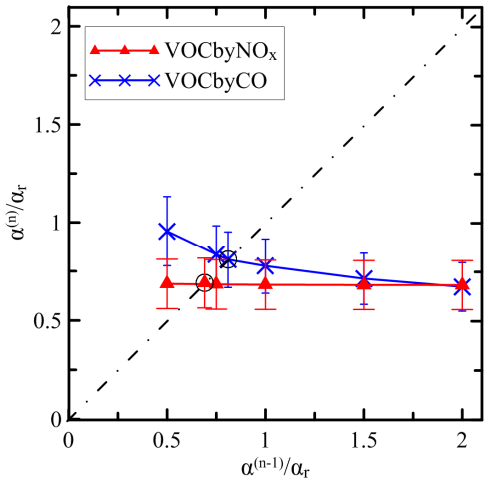

Figure 3. Dependence of the FRP-to-BBR conversion factor values optimized under the assumption of linearity of the relationship between the NO_2 columns and the BB NO_x emission rate on an assumed value of the same conversion factor. The conversion factor values are normalized to their reference value. The dependence is shown for the two estimation cases, "VOCbyNO_x" and "VOCbyCO", see Section 2.2. The estimates circumvented by black circles are the optimal estimates (α_{opt}) obtained as a result of the third iteration (that is, with $n = 3$) of the iterative procedure described in Section 2.2, whereas the other estimates are a result of the initial iteration ($n = 1$).

Another potential source for a bias in our emission estimates is due to uncertainties in estimates of the background estimates of the NO_2 columns. To test the sensitivity of our results to this factor, we repeated our estimation procedure for the VOCbyNO_x case, but with the background NO_2 columns estimated using available observational data for other days (12–14 July 2010 instead of 15–19 July 2010 as in the base case). The optimal estimate of α for the test case was found to be only 10 percent larger than for the base case. This result indicates that our BB NO_x emission estimates are sufficiently robust with regard to random uncertainties in the background NO_2 column amounts. Furthermore, we investigated whether or not the background NO_2 columns changed significantly over the study period (e.g., due to changes in meteorological conditions or in biogenic emission rates). To this end, we selected data points (grid cells and days) where the simulated NO_2 column amounts originated from fires were infinitesimal (less than 10^{-2}% relative to the background NO_2 columns estimated for the same grid cells/days using the OMI data for the period 15–19 July 2010). The selected data were averaged separately over the periods 15–19 July 2010 and 20 July–16 August 2010. As a result, the

mean value over the second period was found to be very insignificantly (~6%) lower than that for the first period. This result confirms that uncertainties in our estimates of α due to uncertainties associated with evaluation of the background NO_2 columns are unlikely to exceed the statistical uncertainties represented by the confidence intervals for the values of α_{opt}.

Figure 4 illustrates the performance of our NO_2 simulation using optimized NO_x emissions for the VOCbyNO_x case. Note that the simulation data for the VOCbyCO case are almost indistinguishable from those in the VOCbyNO_x case and are not presented here. The daily time series shown in Figure 4 are the same as those in Figure 1, except that the BB NO_x emissions used in the simulation presented in Figure 4 were calculated with the optimal estimate of α (α_{opt}) instead of its reference value (α_r) as in Figure 1. Compared to the model results obtained with the reference value of α, the performance of the "optimal" simulation is noticeably better. Specifically, the root mean square error (RMSE) has reduced by more than 20% and a considerable difference (~40%) between the mean values of the NO_2 columns from the model and measurements has practically been eliminated. Furthermore, the absolute values of the differences between the daily values of the NO_2 columns from the measurements and simulations have been reduced in the 19 of 28 days considered (after excluding the initial 5 days used for estimation of the background NO_2 columns). A simple statistical test based on the binomial distribution and involving the statistical hypothesis that our inversion results simply in adding random errors to the simulated NO_2 columns confirms that the improvement of the performance of our NO_2 simulations is statistically significant with the probability of type 1 error being less than 0.05. It is noteworthy that the optimization of the NO_x BB emissions did not affect a value of the correlation coefficient (r). This observation implies that the correlation coefficient in the given case can be considered as an independent (of α) measure of accuracy of the spatial-temporal field of the BB NO_x emissions used in our simulations.

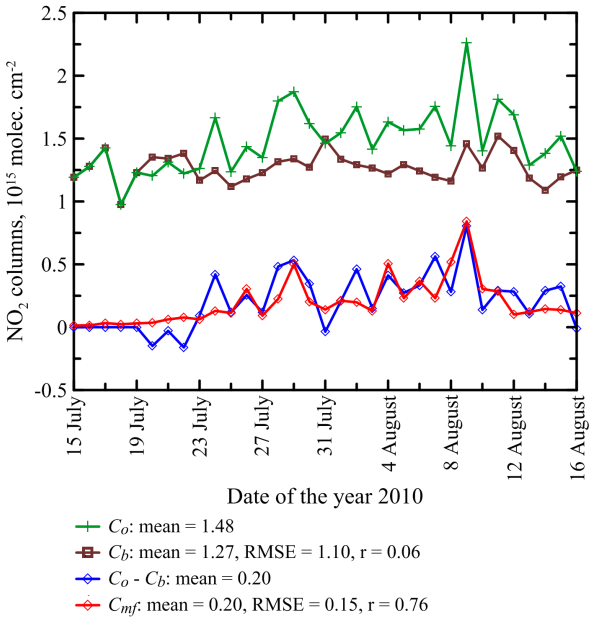

Figure 4. The same as in Figure 1, except that the simulated time series, C_{mf}, was obtained from the model run using the optimal value of the FRP-to-BBR conversion factor for the VOCbyNO_x case.

The spatial distributions of the average (over the study period) NO_2 column amounts obtained using the OMI measurements and given by the CHIMERE model are compared in Figure 5a,b. For the comparison purpose, the simulated BB NO_2 column amounts (C_{mf}) calculated with the optimal estimate of the FRP-to-BBR conversion factor for the VOCbyNO_x case were added to the background values of the NO_2 columns (C_b). Visual comparison of Figure 5a,b reveals that such "composed" data demonstrate a rather reasonable, although evidently imperfect, agreement with the measurement data.

In particular, the both two-dimensional fields of NO_2 columns exhibit the large-scale negative gradients in the north-east direction, as well as the "hot spots" around Moscow. There are also the enhancements in the NO_2 column amounts south of Moscow. Quantitatively, a degree of agreement between the NO_2 columns in the corresponding grid cells can be characterized by the correlation coefficient that is found to be of 0.73. This value indicates that the composed data ($\boldsymbol{C}_{mf} + \boldsymbol{C}_b$) account for about a half of the total variance of the data. The rest of the variance includes, in particular, small scale variability in the both fields, which may partly be due to random uncertainties in $\boldsymbol{C}_o$ and $\boldsymbol{C}_b$. A part of the discrepancies between the composed data and the measurements may also be due to errors in the BB emission data as well as due to the limited spatial coverage of the satellite measurements in the situation considered. For example, one of the prominent discrepancies is that spots with high NO_2 columns east of Moscow at approximately 45°E in Figure 5b,c (which, according to our additional analysis, are mostly due to strong emissions from fires on 26 July) are missing in Figure 5a. This discrepancy may be due to, e.g., mismatches between the MODIS and OMI measurement in space and time: that is, the smoke plumes from the fire spots which were "seen" by the MODIS instruments could be outside the "vision field" of the OMI instrument (at least partly). Nonetheless, the reasonable overall agreement between the data shown in Figure 5a,b provides one more argument in favor of reliability of the results of our analysis. Note that, in accordance to our results shown in Figure 4, a contribution of fires to the tropospheric NO_2 columns is found to be relatively small (see Figure 5c).

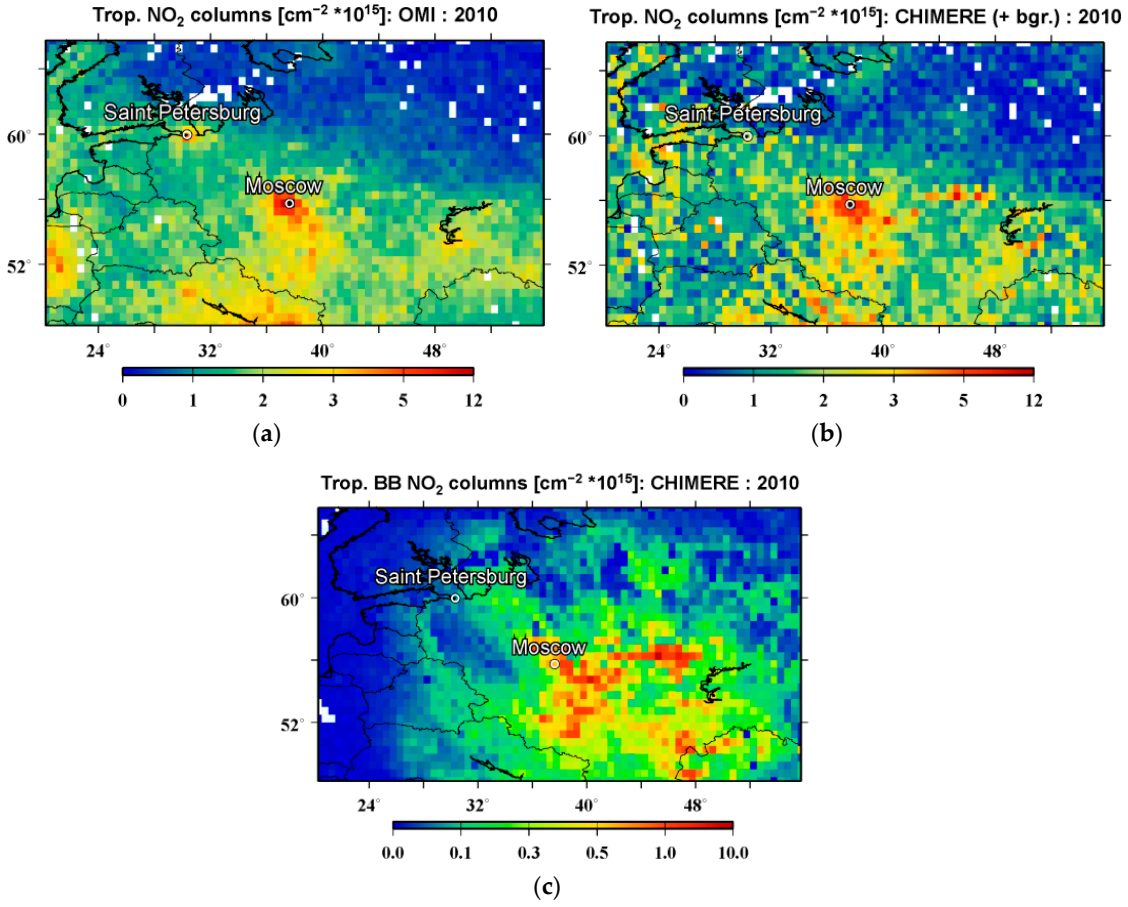

Figure 5. The spatial distributions of the average (over the study period) NO_2 column amounts obtained using the OMI measurements (**a**); The modeled data that were composed by summing up the simulated tropospheric column amounts of NO_2 from fires and the background values of the tropospheric NO_2 columns (**b**); and The simulated tropospheric column amounts of NO_2 from fires (**c**) are also shown separately.

3.2. NO_x Lifetime Estimates

The NO_x lifetime estimates (τ_{nox}) obtained in accordance to Equation (5) are presented in Figure 6 as a function of α for the two estimation cases ("VOCbyNO$_x$" and "VOCbyCO"). Similar to the dependencies of $\alpha^{(n)}$ on $\alpha^{(n-1)}$ that are shown in Figure 3, the dependencies of τ_{nox} on α for the two cases are qualitatively different. Specifically, while the case "VOCbyNO$_x$" features almost constant NO_x lifetimes irrespectively of the assumed values of the conversion factor, the values of τ_{nox} obtained for the "VOCbyCO" case are increasing by a factor of 2.1 with the increase of α by a factor of 4. The NO_x lifetime values corresponding to the optimal estimates of the conversion factor are 4.2 and 3.1 h for the "VOCbyNO$_x$" and "VOCbyCO" cases. These values are within a rather broad range of lifetimes (2–6 h) assumed in earlier studies of BB NO_x emissions [11–14].

Importantly, the relative difference between the lifetimes calculated for the "VOCbyNO$_x$" and "VOCbyCO" cases is much larger compared to the relative difference between values of α_{opt} (see Figure 3) for the same cases. As mentioned above (see Section 3.1), our estimates of α depend on the ratio of the mean BB NO_2 column amounts and NO_x emissions. Since this ratio depends not only on the NO_x lifetime but also on the NO_2/NO ratio, a comparison of the results shown in Figures 3 and 6 indicates that the difference of the lifetimes is counterbalanced by the difference of the NO_2/NO ratio.

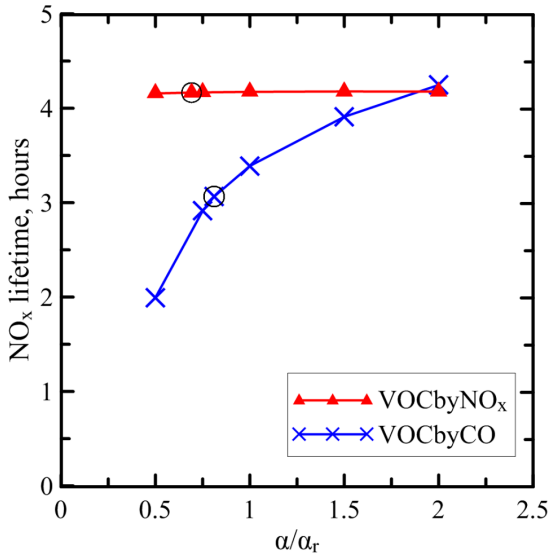

Figure 6. The effective NO_x lifetime (τ_{nox}) estimated a function of the FRP-to-BBR conversion factor (α) normalized to its reference value (α_r). Black circles depict the NO_x lifetime values corresponding to the optimal estimates of α for the two estimation cases ("VOCbyNO$_x$" and "VOCbyCO") considered in this study.

Exhaustive theoretical interpretation of the dependencies shown in Figure 6 goes beyond the scope of this study. Here, we discuss the chemical mechanisms underlying these dependencies only very briefly. In particular, we note that NO_x is mainly removed from the atmosphere in a reaction of NO_2 with OH [1]. Both OH and NO_2 concentrations are typically growing functions of ozone (O_3) concentration [1]. Our simulation data for O_3 and OH concentrations (not presented here) indicate that "hot spots" featuring strong BB emissions typically coincide in space and time with depleted concentrations of these species, as well as with reduced values of NO_2/NO ratio. It can be speculated that the behavior of the O_3 formation rate is the main factor determining a nearly linear dependence of NO_2 concentration on the BB NO_x emission rate over the hot spots. Specifically, in the "high NO_x limit" (in which OH concentration is relatively small), the O_3 formation rate is known to be proportional to the ratio of VOC to NO_x concentrations [1] and thus can be expected to be independent of α in the

"VOCbyNO$_x$" case. In contrast, the VOC emission rate is independent of α in the "VOCbyCO" case. Thus the O_3 formation rate is likely to decrease with an increase of α, leading to the observed increase in the NO_x lifetime.

Such an interpretation of the results presented in Figure 6 is consistent with the dependencies presented in Figure 3. Indeed, given that the NO_x lifetime is almost independent of α in the "VOCbyNO$_x$", the results shown in Figure 3 for the same case imply that the NO_2/NO ratio and thus O_3 concentration are also kept nearly constant. On the other hand, the fact that the relative range of the changes of $\alpha^{(n)}$ in the "VOCbyCO" case in Figure 3 is much smaller than that of the changes of τ_{nox} in Figure 6 indicates that the NO_2/NO ratio decreases with an increase of α in that case: this observation, in turn, implies that O_3 concentration accordingly decreases.

3.3. NO_x Emission Estimates

We used our optimal estimate of the FRP-to-BBR conversion factor (0.254 kg·s^{-1}·MW^{-1}) for the VOCbyNO$_x$ case to calculate NO_x emission rates from wildfires in the study region and period. Figure 7 shows the time series of the daily BB NO_x emission rates that were obtained by integrating either over all grid cells and hours of a given day or only over selected grid cells/hours that were provided with the OMI NO_2 data. According to our calculations, the "full" emissions tended to increase until 6 August and then started to decrease, consistently with results of other studies [9,19,21,49] that reported on the strong air pollution in the study region in the beginning of August. Two major peaks of the BB NO_x emission rate occurred on 4 August and 6 August. A difference between the two time series indicates to what extent the information provided by the OMI retrievals on BB NO_x emissions is representative of the whole study period. Evidently, the BB NO_x emission rates corresponding to the scenes provided with the OMI NO_2 retrievals represent only a part (around 30%, on the average) of the integral emission rates in the study region and period. Therefore, there is a question whether or not our optimal estimate of the FRP-to-BBR conversion factor is representative (at least, on average) of all fires in the study region.

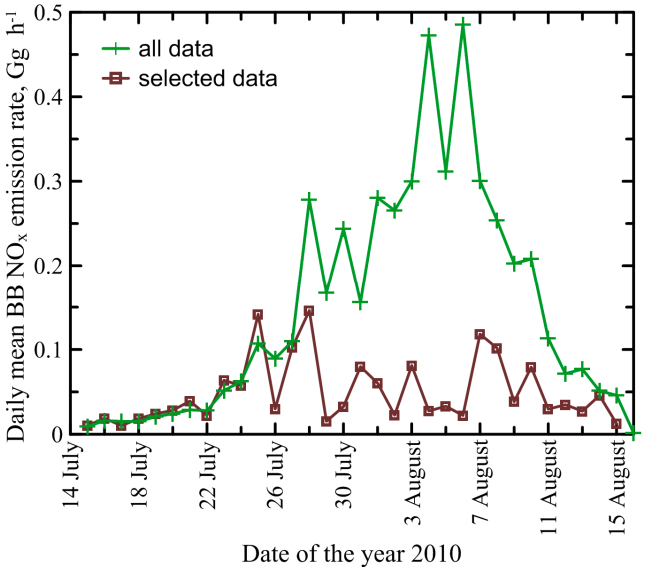

Figure 7. Time series of the daily mean BB NO_x emission rates that were obtained by integrating either over all model grid cells (see the green curve) or only over selected grid cells that are provided with the OMI NO_2 data for a given day (see the brown curve).

Figure 8 presents the spatial distributions of the BB NO_x emission rates averaged over the study period. The two different distributions (shown in Figure 8a,b) correspond to the two respective time series presented in Figure 7. Expectedly, the distribution obtained only with the selected data typically

features smaller BB NO_x emission rates compared to the one obtained using all the available emission data. Nonetheless, it is important to note that both the coverage and spatial structure of the emission rates shown in the different distributions are rather similar. In particular, both distributions show that there were strong NO_x emissions from fires in the regions south-east and east of Moscow as well as around Russia's border with Kazakhstan (near the bottom right-hand corner of the model domain). Furthermore, only 9% of the fire spots (grid cells with non-zero fire emissions) shown in Figure 8a are missing in Figure 8b. Therefore, a comparison of the spatial distributions shown in Figure 8a,b provide evidence that our optimal conversion factor estimate that was used to scale BB NO_x emissions rates across the study region is, to a considerable extent, representative of the whole region and period considered. Note that, according to a special test involving splitting the study period into two approximately equal parts, the difference between the optimal values of the conversion factor for those periods was less than the statistical uncertainty of our estimate for the whole period. Although the result of this test provides further evidence in favor of applicability of our optimal conversion factor estimates across the study region and period, the question regarding the representativeness of the conversion factor estimates derived from observations of the limited number of fire scenes still remains and requires further investigations that go beyond of the scope of this study.

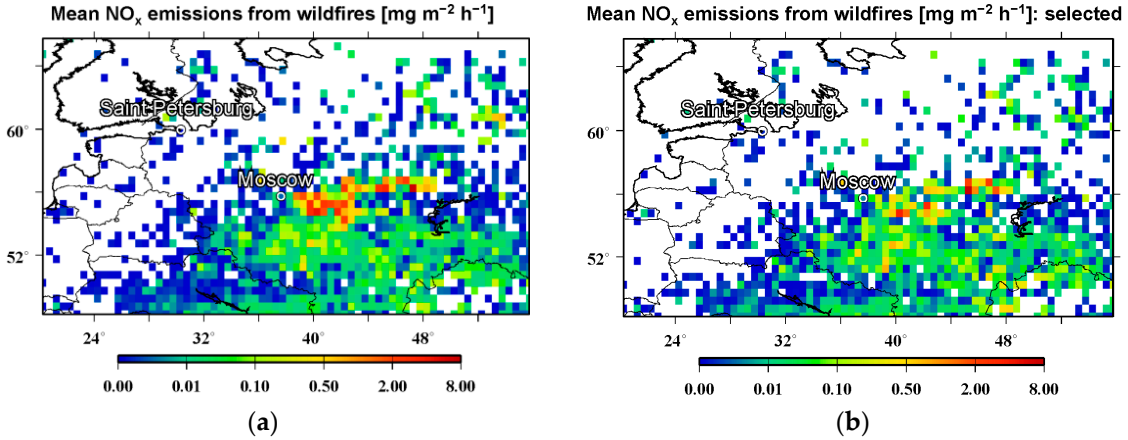

Figure 8. Spatial distributions of the BB NO_x emission rates averaged over the study period. The two different distributions are obtained by averaging either over all model grid cells and hours in the study period (**a**); or only those grid cells/hours which are provided with the OMI NO_2 retrievals (**b**) and correspond to the green and brown curves in Figure 7, respectively.

Figure 9 compares our estimates of the total BB NO_x emissions in the study region and period with corresponding estimates obtained using the data of fire emission inventories, such as GFED4.1s [8] and GFASv1.0 [9]. The GFED inventory is based on satellite measurements of burned area and other parameters from a biosphere model, while the GFAS inventory infers BB emissions from the FRP satellite measurements by using a method similar to one employed in this study. However, unlike our method, where the conversion factor is optimized against atmospheric composition measurements, the GFAS inventory uses conversion factor values calibrated with the GFED data. Thus the GFED4.1s and GFASv1.0 inventories are not fully independent, although the spatial structure and temporal variability of regional emission fields provided by these inventories may be significantly different. Our results suggest that both GFED4.1s and GFASv1.0 considerably underestimate BB NO_x emissions (by 33% and 30%, respectively, relative to our estimate for the VOCbyNO$_x$ case) and that the difference between our emission estimate and the respective inventory data cannot be explained by statistical uncertainties in our estimates. This finding is qualitatively consistent with the results of other studies (see, e.g., [19–21,36]) where those inventories were found to underestimate emissions of other species (such as CO and aerosol) from wildfires in Russia. It should be kept in mind, however, that the confidence intervals shown in Figure 9 may not fully account for possible biases in our estimates

due to several factors mentioned above, including uncertainties in the VOC BB emissions and in background NO_2 column amounts, probable negative biases in the satellite NO_2 retrievals for the strongly polluted scenes, possible inconsistencies between the NO_2 vertical profiles used in the retrieval and predicted by our model, as well as possibly insufficient spatial and temporal representativeness of the observational constraints provided by the available NO_2 satellite measurements to BB NO_x emissions. Quantitative understanding of these factors and their impacts on BB NO_x emission estimates inferred from satellite NO_2 measurements calls for further dedicated studies.

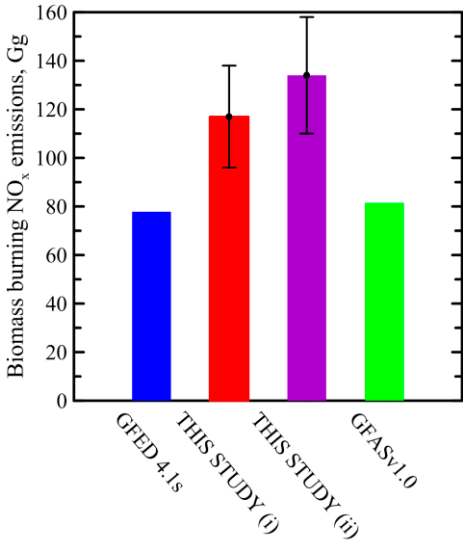

Figure 9. Optimal estimates of the total NO_x emissions in the study region and period in comparison with corresponding estimates based on the data of the GFED4.1s and GFASv1.0 emission inventories. The optimal estimates are shown separately for the two estimation cases, "VOCbyNO_x" (i) and "VOCbyCO" (ii). The confidence intervals represent statistical uncertainty evaluated in terms of the 95th percentile.

4. Conclusions

In this paper, we examined the feasibility of estimating NO_x emissions from wildfires within an inverse modeling approach by using satellite measurements of NO_2 columns. For this purpose, we considered the situation of the mega-fire event that occurred in the European part of Russia in July–August 2010. We used the tropospheric NO_2 columns available from satellite measurements performed with the OMI instrument along with the NO_2 column amounts simulated with the CHIMERE chemistry transport model (CTM) in which emissions of NO_x and other species from biomass burning (BB) were taken into account. The BB emissions were calculated using the Fire Radiative Power (FRP) data that were available from the MODIS satellite instrument. The measured and simulated NO_2 columns were combined in the framework of a simple inverse modeling method aimed at estimating the conversion factor (α) from FRP to BB rate. BB emissions of individual model species were then calculated using estimates of α and typical emission factors reported in literature.

The focus in our study was given to analysis of the effect of chemical nonlinearities on the relationship between BB NO_x emissions and respective NO_2 column amounts. While in our study this relationship was simulated with CTM, several previous studies (mentioned in the Introduction) in which BB NO_x emissions had been investigated using NO_2 OMI measurements, involved explicit quantitative assumptions regarding the dependence of NO_2 columns on BB NO_x emissions. To test the robustness of such assumptions, we performed several model runs where a typical "reference" value of the conversion factor (and thus the mean BB NO_x emission rate) was scaled with a factor ranging from 0.5 to 2.0. The simulations were done for the two cases involving different assumptions

regarding emissions of volatile organic compounds (VOCs) and CO. Specifically, in one of the cases ("VOCbyNO_x"), VOCs and CO emission rates were scaled in the same way as the NO_x emissions, while in another case ("VOCbyCO"), the VOCs and CO emission rates were calculated with the α value inferred in a previous study from ground-based measurements of CO and were kept constant irrespectively of changes in the NO_x emission rates. The corresponding linearized relationships (predicted by the model) between the NO_2 columns and BB NO_x emission rate were used to obtain optimal estimates of α. Furthermore, using results of the same model runs, we evaluated the effective NO_x lifetime.

It is found that the available measurement data and simulations yield a reasonable estimate of the conversion factor with a statistical uncertainty (evaluated in terms of the 95th percentile) of about $\pm$20%. The optimal value of the conversion factor for the VOCbyNO_x case is estimated to be ~0.25 kg s^{-1}·MW^{-1}. This value is about 30% smaller than the respective "reference" estimate (of 0.368 kg·s^{-1}) obtained earlier in a laboratory experiment. The optimal estimate for the VOCbyCO case is found to be about 15% larger compared to the estimate for the VOCbyNO_x case. Note that the differences between the reference and our estimates of the conversion factor may, in principle, compensate for biases in the NO_x emission factors specified in our simulations, since our emission model involves a multiplicative combination of both factors.

Our results indicate that chemical nonlinearities may have considerably different effects on the relationship between BB NO_x emissions and NO_2 columns, depending on an assumed ratio of the NO_x and VOC emission rates. Specifically, in the VOCbyNO_x case, where that ratio was kept constant, both the NO_2 columns-NO_x emissions relationship and the effective NO_x lifetime were found to be almost independent of variations of an assumed value of the conversion factor α. The effective NO_x lifetime for this case was estimated to be ~4.2 h which is within a broad range of NO_x lifetimes (2–6 h) assumed in previous studies [11–14]. In contrast, in the VOCbyCO case, both the BB NO_2 columns/BB NO_x emission rate ratio and the effective NO_x lifetime were found to substantially increase with an increase of the NO_x emission rate (scaled uniformly with α). In particular, the effective NO_x lifetime was found to increase from ~2.0 to 4.2 h as the conversion factor used in our simulations increased from 0.184 to 0.736 kg·s^{-1}·MW^{-1}. These results imply that in a common case where the BB VOC emission rates are not constrained by respective measurements, the NO_x lifetime (as well as the relationship between the NO_2 columns and BB NO_x emission rates) remains, to some extent, uncertain and the effects of chemical nonlinearities on BB NO_x emission estimates cannot be "a priori" disregarded.

The optimized values of the conversion factors were used to estimate the total NO_x amount emitted from wildfires in the study region in the period from 15 July to 16 August. Our estimates are found to be at least a factor of 1.4 larger compared to the corresponding values predicted by the GFED4.1s and GFASv1.0 fire emission inventories. The differences between our estimates and the inventory data considerably exceed the statistical confidence intervals of our estimates. This result suggests that both of the inventories are likely to underestimate NO_x emissions from the Russian 2010 wildfires. However, it should be noted that the statistical confidence intervals for our emission estimates do not necessarily account for all kinds of systematic uncertainties in measurement and simulation data used in our analysis. Such uncertainties may include those in the BB VOC emissions, in background NO_2 column amounts, probable negative biases in satellite NO_2 retrievals for the strongly polluted scenes, as well as biases due to limited spatial and temporal coverage of available NO_2 satellite measurements. Evaluation of these uncertainties goes beyond the scope of this study and should be addressed in future studies. Nonetheless, even in view of the probable uncertainties, we believe that our independent BB NO_x emission estimates constrained by satellite measurements are a useful contribution to a practically important research direction dealing with the evaluation of BB emissions, especially taking into account that available data provided by fire emission inventories may also be subject to various poorly known uncertainties.

Acknowledgments: This study was supported by the Russian Foundation for Basic Research (grant No. 14-05-00481 and 15-45-02516). Development of the estimation method used in this study was supported

by the Russian Science Foundation (grant agreement No. 15-17-10024). The authors acknowledge the free use of tropospheric NO_2 column data from the OMI sensor from www.temis.nl.

Author Contributions: E.V. Berezin performed simulations and created computer programs used in the analysis. I.B. Konovalov conceived the method of the analysis and wrote the paper, Y.Y. Romanova contributed to the analysis of the simulation and measurement data and to the technical preparation of the paper.

Conflicts of Interest: The authors declare no conflict of interest. The founding sponsors had no role in the design of the study; in the collection, analyses, or interpretation of data; in the writing of the manuscript, and in the decision to publish the results.

References

1. Seinfeld, J.H.; Pandis, S.N. Chemistry of the troposphere. In *Atmospheric Chemistry and Physics: From Air Pollution to Climate Change*, 2nd ed.; John Wiley & Sons, Inc.: New York, NY, USA, 2006; pp. 204–230.
2. Monks, P.S. Gas-phase radical chemistry in the troposphere. *Chem. Soc. Rev.* **2005**, *34*, 376–395. [CrossRef] [PubMed]
3. Konovalov, I.B. Nonlinear relationships between atmospheric aerosol and its gaseous precursors: Analysis of long-term air quality monitoring data by means of neural networks. *Atmos. Chem. Phys.* **2003**, *3*, 607–621. [CrossRef]
4. Ng, N.L.; Chhabra, P.S.; Chan, A.W.H.; Surratt, J.D.; Kroll, J.H.; Kwan, A.J.; McCabe, D.C.; Wennberg, P.O.; Sorooshian, A.; Murphy, S.M.; et al. Effect of NO_x level on secondary organic aerosol (SOA) formation from the photooxidation of terpenes. *Atmos. Chem. Phys.* **2007**, *7*, 5159–5174. [CrossRef]
5. Jaeglé, L.; Steinberger, L.; Martin, R.V.; Chance, K. Global partitioning of NO_x sources using satellite observations: Relative roles of fossil fuel combustion, biomass burning and soil emissions. *Faraday Discuss.* **2005**, *130*, 407–423. [CrossRef] [PubMed]
6. Jaffe, D.A.; Wigder, N.L. Ozone production from wildfires: A critical review. *Atmos. Environ.* **2012**, *51*, 1–10. [CrossRef]
7. Mebust, A.K.; Russell, A.R.; Hudman, R.C.; Valin, L.C.; Cohen, R.C. Characterization of wildfire NO_x emissions using MODIS fire radiative power and OMI tropospheric NO_2 columns. *Atmos. Chem. Phys.* **2012**, *11*, 5839–5851. [CrossRef]
8. Randerson, J.T.; van der Werf, G.R.; Giglio, L.; Collatz, G.J.; Kasibhatla, P.S. *Global Fire Emissions Database*, Version 4, (GFEDv4); ORNL DAAC: Oak Ridge, TN, USA, 2015.
9. Kaiser, J.W.; Heil, A.; Andreae, M.O.; Benedetti, A.; Chubarova, N.; Jones, L.; Morcrette, J.-J.; Razinger, M.; Schultz, M.G.; Suttie, M.; et al. Biomass burning emissions estimated with a global fire assimilation system based on observed fire radiative power. *Biogeosciences* **2012**, *9*, 527–554. [CrossRef]
10. Akagi, S.K.; Yokelson, R.J.; Wiedinmyer, C.; Alvarado, M.J.; Reid, J.S.; Karl, T.; Crounse, J.D.; Wennberg, P.O. Emission factors for open and domestic biomass burning for use in atmospheric models. *Atmos. Chem. Phys.* **2011**, *11*, 4039–4072. [CrossRef]
11. Mebust, A.K.; Cohen, R.C. Space-based observations of fire NO_x emission coefficients: A global biome-scale comparison. *Atmos. Chem. Phys.* **2014**, *14*, 2509–2524. [CrossRef]
12. Schreier, S.F.; Richter, A.; Kaiser, J.W.; Burrows, J.P. The empirical relationship between satellite-derived tropospheric NO_2 and fire radiative power and possible implications for fire emission rates of NO_x. *Atmos. Chem. Phys.* **2014**, *14*, 2447–2466. [CrossRef]
13. Tanimoto, H.K.; Ikeda, K.F.; Boersma, R.J.; van der Garivait, A.S. Interannual variability of nitrogen oxides emissions from boreal fires in Siberia and Alaska during 1996–2011 as observed from space. *Environ. Res. Lett.* **2015**, *10*, 065004. [CrossRef]
14. Schreier, S.F.; Richter, A.; Schepaschenko, D.; Shvidenko, A.; Hilboll, A.; Burrows, J.P. Differences in satellite-derived NOx emission factors between Eurasian and North American boreal forest fires. *Atmos. Environ.* **2015**, *121*, 55–65. [CrossRef]
15. Konovalov, I.B.; Beekmann, M.; Richter, A.; Burrows, J.P. Inverse modelling of the spatial distribution of NO_x emissions on a continental scale using satellite data. *Atmos. Chem. Phys.* **2006**, *6*, 1747–1770. [CrossRef]
16. Miyazaki, K.; Eskes, H.J.; Sudo, K. Global NO_x emission estimates derived from an assimilation of OMI tropospheric NO_2 columns. *Atmos. Chem. Phys.* **2012**, *12*, 2263–2288. [CrossRef]
17. Mijling, B.; van der A, R.J. Using daily satellite observations to estimate emissions of short-lived air pollutants on a mesoscopic scale. *J. Geophys. Res. Atmos.* **2012**, *117*, D17302. [CrossRef]

18. Berezin, E.V.; Konovalov, I.B.; Ciais, P.; Richter, A.; Tao, S.; Janssens-Maenhout, G.; Beekmann, M.; Schulze, E.-D. Multiannual changes of CO_2 emissions in China: Indirect estimates derived from satellite measurements of tropospheric NO_2 columns. *Atmos. Chem. Phys.* **2013**, *13*, 9415–9438. [CrossRef]
19. Konovalov, I.B.; Beekmann, M.; Kuznetsova, I.N.; Yurova, A.; Zvyagintsev, A.M. Atmospheric impacts of the 2010 Russian wildfires: Integrating modelling and measurements of an extreme air pollution episode in the Moscow region. *Atmos. Chem. Phys.* **2011**, *11*, 10031–10056. [CrossRef]
20. Krol, M.; Peters, W.; Hooghiemstra, P.; George, M.; Clerbaux, C.; Hurtmans, D.; McInerney, D.; Sedano, F.; Bergamaschi, P.; El Hajj, M.; et al. How much CO was emitted by the 2010 fires around Moscow? *Atmos. Chem. Phys.* **2013**, *13*, 4737–4747. [CrossRef]
21. Konovalov, I.B.; Beekmann, M.; Berezin, E.V.; Petetin, H.; Mielonen, T.; Kuznetsova, I.N.; Andreae, M.O. The role of semi-volatile organic compounds in the mesoscale evolution of biomass burning aerosol: A modeling case study of the 2010 mega-fire event in Russia. *Atmos. Chem. Phys.* **2015**, *15*, 13269–13297. [CrossRef]
22. Levelt, P.F.; Hilsenrath, E.; Leppelmeier, G.W.; van den Oord, G.H.J.; Bhartia, P.K.; Tamminen, J.; de Haan, J.F.; Veefkind, J.P. Science objectives of the ozone monitoring instrument. *IEEE Trans. Geosci. Remote Sens.* **2006**, *44*, 1199–1208. [CrossRef]
23. Boersma, K.F.; Eskes, H.J.; Dirksen, R.J.; van der A, R.J.; Veefkind, J.P.; Stammes, P.; Huijnen, V.; Kleipool, Q.L.; Sneep, M.; Claas, J.; et al. An improved tropospheric NO_2 column retrieval algorithm for the Ozone Monitoring Instrument. *Atmos. Meas. Tech.* **2011**, *4*, 1905–1928. [CrossRef]
24. TEMIS Portal. Available online: http://www.temis.nl/ (accessed on 17 March 2016).
25. Irie, H.; Boersma, K.F.; Kanaya, Y.; Takashima, H.; Pan, X.; Wang, Z.F. Quantitative bias estimates for tropospheric NO_2 columns retrieved from SCIAMACHY, OMI, and GOME-2 using a common standard for East Asia. *Atmos. Meas. Tech.* **2012**, *5*, 2403–2411. [CrossRef]
26. Boersma, K.F.; Eskes, H.J.; Brinksma, E.J. Error analysis for tropospheric NO_2 retrieval from space. *J. Geophys. Res. Atmos.* **2004**, *109*, D04311. [CrossRef]
27. Kaufman, Y.J.; Justice, C.O.; Flynn, L.P.; Kendall, J.D.; Prins, E.M.; Giglio, L.; Ward, D.E.; Menzel, W.P.; Setzer, A.W. Potential global fire monitoring from EOS-MODIS. *J. Geophys. Res.* **1998**, *103*, 32215–32238. [CrossRef]
28. Justice, C.O.; Giglio, L.; Korontzi, S.; Owens, J.; Morisette, J.T.; Roy, D.; Descloitres, J.; Alleaume, S.; Petitcolin, F.; Kaufman, Y. The MODIS fire products. *Remote Sens. Environ.* **2002**, *83*, 244–262. [CrossRef]
29. The NASA Land Processes Distributed Active Archive Center. Available online: https://lpdaac.usgs.gov (accessed on 14 June 2015).
30. Remer, L.A.; Kaufman, Y.J.; Tanre, D.; Mattoo, S.; Chu, D.A.; Martins, J.V.; Li, R.-R.; Ichoku, C.; Levy, R.C.; Kleidman, R.G.; et al. The MODIS aerosol algorithm, products, and validation. *J. Atmos. Sci.* **2005**, *62*, 947–973. [CrossRef]
31. The NASA Giovanni-Interactive Visualization and Analysis System. Available online: http://daac.gsfc.nasa.gov/giovanni/ (accessed on 23 June 2014).
32. Menut, L.; Bessagnet, B.; Khvorostyanov, D.; Beekmann, M.; Blond, N.; Colette, A.; Coll, I.; Curci, G.; Foret, G.; Hodzic, A.; et al. CHIMERE 2013: A model for regional atmospheric composition modeling. *Geosci. Model Dev.* **2013**, *6*, 981–1028. [CrossRef]
33. The CHIMERE Chemistry-Transport Model. Available online: http://www.lmd.polytechnique.fr/chimere/ (accessed on 30 June 2016).
34. Hodzic, A.; Madronich, S.; Bohn, B.; Massie, S.; Menut, L.; Wiedinmyer, C. Wildfire particulate matter in Europe during summer 2003: Meso-scale modeling of smoke emissions, transport and radiative effects. *Atmos. Chem. Phys.* **2007**, *7*, 4043–4064. [CrossRef]
35. Konovalov, I.B.; Beekmann, M.; D'Anna, B.; George, C. Significant light induced ozone loss on biomass burning aerosol: Evidence from chemistry-transport modeling based on new laboratory studies. *Geophys. Res. Lett.* **2012**, *39*. [CrossRef]
36. Konovalov, I.B.; Berezin, E.V.; Ciais, P.; Broquet, G.; Beekmann, M.; Hadji-Lazaro, J.; Clerbaux, C.; Andreae, M.O.; Kaiser, J.W.; Schulze, E.-D. Constraining CO_2 emissions from open biomass burning by satellite observations of co-emitted species: A method and its application to wildfires in Siberia. *Atmos. Chem. Phys.* **2014**, *14*, 10383–10410. [CrossRef]

37. Wooster, M.J.; Roberts, G.; Perry, G.L.W.; Kaufman, Y.J. Retrieval of biomass combustion rates and totals from fire radiative power observations: FRP derivation and calibration relationships between biomass consumption and fire radiative energy release. *J. Geophys. Res.* **2005**, *110*, D24311. [CrossRef]
38. Sofiev, M.; Ermakova, T.; Vankevich, R. Evaluation of the smoke-injection height from wild-land fires using remote-sensing data. *Atmos. Chem. Phys.* **2012**, *12*, 1995–2006. [CrossRef]
39. Madronich, S.; McKenzie, R.E.; Bjorn, L.O.; Caldwell, M.M. Changes in biologically active ultraviolet radiation reaching the earth's surface. *J. Photochem. Photobiol. B Biol.* **1998**, *46*, 5–19. [CrossRef]
40. Skamarock, W.C.; Klemp, J.B.; Dudhia, J.; Gill, D.O.; Barker, D.M.; Duda, M.G.; Huang, X.-Y.; Wang, W.; Powers, J.G. *A Description of the Advanced Research WRF*, Version 3; NCAR Tech. Notes-475CSTR; National Center for Atmospheric Research: Boulder, CO, USA, 2008; p. 113.
41. Eskes, H.J.; Boersma, K.F. Averaging kernels for DOAS total column satellite retrievals. *Atmos. Chem. Phys.* **2003**, *3*, 1285–1291. [CrossRef]
42. Konovalov, I.B.; Beekmann, M.; Vautard, R.; Burrows, J.P.; Richter, A.; Elansky, N.; Nüß, H. Comparison and evaluation of modelled and GOME measurement derived tropospheric NO_2 columns over Western and Eastern Europe. *Atmos. Chem. Phys.* **2005**, *5*, 169–190. [CrossRef]
43. Konovalov, I.B.; Elansky, N.F.; Zvyagintsev, A.M.; Belikov, I.B.; Beekmann, M. Validation of chemistry transport model of the lower atmosphere in the central European region of Russia using ground-based and satellite measurement data. *Russ. Meteorol. Hydrol.* **2009**, *34*, 236–242. [CrossRef]
44. Efron, B.; Tibshirani, R.J. *An Introduction to the Bootstrap*; Chapman & Hall: New York, NY, USA, 1993.
45. Boersma, K.F.; Eskes, H.J.; Veefkind, J.P.; Brinksma, E.J.; van der A, R.J.; Sneep, M.; van den Oord, G.H.J.; Levelt, P.F.; Stammes, P.; Gleason, J.F.; et al. Near-real time retrieval of tropospheric NO_2 from OMI. *Atmos. Chem. Phys.* **2007**, *7*, 2103–2118. [CrossRef]
46. Seinfeld, J.H.; Pandis, S.N. Atmospheric Trace Constituents. In *Atmospheric Chemistry and Physics: From Air Pollution to Climate Change*, 2nd ed.; John Wiley & Sons, Inc.: New York, NY, USA, 2006; pp. 22–24.
47. Matsueda, M. Predictability of Euro-Russian blocking in summer of 2010. *Geophys. Res. Lett.* **2011**, *38*, L06801. [CrossRef]
48. Andreae, M.O.; Merlet, P. Emission of trace gases and aerosols from biomass burning. *Glob. Biogeochem. Cycles* **2001**, *15*, 955–966. [CrossRef]
49. Huijnen, V.; Flemming, J.; Kaiser, J.W.; Inness, A.; Leitão, J.; Heil, A.; Eskes, H.J.; Schultz, M.G.; Benedetti, A.; Hadji-Lazaro, J.; et al. Hindcast experiments of tropospheric composition during the summer 2010 fires over western Russia. *Atmos. Chem. Phys.* **2012**, *12*, 4341–4364. [CrossRef]